NOTES AND CORRESPONDENCE

On Triad Interactions in a Linearly Stratified Ocean

CHING-LONG LIN, JEFFREY R. KOSEFF, AND JOEL H. FERZIGER

Environmental Fluid Mechanics Laboratory, Department of Civil Engineering, Stanford University, Stanford, California

8 November 1993 and 22 March 1994

ABSTRACT

Triad interactions in a linearly stratified ocean are studied numerically using a Garrett–Munk energy spectrum as the initial condition. It is found by bispectrum analysis that wave–mean flow interactions dominate and resonant interactions are limited to very large scales. Resonant triads of parametric subharmonic instability type play an insignificant role in the energy distribution. Local sum resonant triads provide the most effective energy transfer at very large scales. The analysis of triadic energy transfer rates suggests that triad configuration determines the energy flow pattern. When the modes with zero horizontal wavenumber are set to zero, resonant interactions arise. Thus, over most of the Garrett–Munk spectrum the energy level is low enough for resonance, but due to strong nonlinearities induced by horizontal currents, resonance is destroyed and wave–mean flow interactions dominate. If the energy level is reduced by a factor of 100, the number of resonant modes increases but wave–mean flow interactions remain important at high wavenumber.

1. Introduction

The triad resonant interaction is believed by some to be the dominant energy transfer mechanism in the ocean; for instance, see Phillips (1977), McComas and Bretherton (1977), Garrett and Munk, (1979) and Munk (1981). Holloway (1980, 1982), however, disagrees and argues that oceanic waves are too energetic for weak resonant interaction theory to apply. Flatté et al. (1985) found that, in contrast to the induced diffusion weak resonant mechanism described by McComas and Bretherton (1977), small-scale internal waves evolve toward higher frequencies and higher horizontal wavenumber. A complete review of our knowledge of nonlinear interactions among oceanic internal waves is given in Müller et al. (1986). Although resonant triads have been identified experimentally (Martin et al. 1972) and numerically (Lin 1993), they were generated in controlled environments.

Efforts to verify whether or not resonance occurs in the ocean were made by McComas and Bretherton (1977), McComas and Müller (1981), and Holloway (1980, 1982). The ratio of the interaction timescale (or the spectral evolution time) to the wave period needs to be very large for weak interaction theory to apply. Holloway (1980, 1982) questioned the validity of the timescale ratio calculated by McComas (1977) and recalculated it; his results contradict the long interaction time assumption. Holloway (1980) further estimated that the oceanic wave energy level is about one hundred times the limit at which weak interaction theory should apply. In addition, Holloway (1983) proposed that large-scale oceanic internal waves (60–100 m or larger) can be treated by resonant interaction theory while interactions between very different length scales, that is, induced diffusion (McComas and Bretherton 1977), are not sensitive to energy level and may be strong in the ocean. The goal of this work is then to obtain evidence for resonance, or lack thereof, in the ocean and to discuss energy transfer mechanisms other than resonant interactions.

To achieve this goal an approach different from previous work, such as McComas and Bretherton (1977), Holloway (1980, 1982), Pomphrey et al. (1980), and Flatté et al. (1985), is adopted. In the cited work, the energy spectrum is based on a semi-empirical oceanic spectrum suggested by Garrett and Munk (1972, 1975, 1979) and Munk (1981). Pomphrey et al. (1980) used Langevin methods to confirm the conclusions of McComas and Bretherton (1977) that the Garrett–Munk (GM) spectrum with a linear density profile is approximately a steady-state spectrum, while Flatté et al. (1985) adopted the Eikonal technique to show that small-scale internal waves evolve toward higher frequencies in contrast to the results predicted by a simple induced-diffusion weak interaction model (see also Müller et al. 1986). In McComas and Bretherton (1977) and Holloway (1980, 1982), the energy transfer equation used to calculate the timescale ratio is derived from the weak interaction equation by Hasselmann

Corresponding author address: Dr. Jeffrey R. Koseff, Department of Civil Engineering, Stanford University, Stanford, CA 94305-4020.

(1966). The wave energy level can strongly affect the applicability of resonant interaction concepts to the ocean. Hasselmann (1966) invoked concepts from quantum mechanics and assumed a Gaussian phase distribution to derive a wave action equation that has been used by Olbers (1976), McComas and Bretherton (1977), and McComas and Müller (1981), among others, to study oceanic dynamics. However, the stability criterion derived from Hasselmann's (1967) weak interaction theory gave poor agreement with the results of single triad analysis (Lin et al. 1993a) and numerical experiments at high wavenumbers (Lin 1993), implying that the timescale ratio calculated from his energy transfer equation is not accurate, especially for finite-amplitude waves. Holloway (1982) also questioned the applicability of Hasselmann's theory to finite-amplitude waves.

In the present study, direct numerical simulations using the Garrett–Munk energy spectrum as the initial condition are performed. A similar approach has been used by Shen and Holloway (1986), Ramsden and Holloway (1992), and Siegel (1990). In the first study, a spectrum similar to the Garrett–Munk spectrum was used to study nonlinear internal wave behavior in the ocean; it showed that the high wavenumber modes have large frequency fluctuations but the dominant resonant and nonresonant triads were not discussed. Ramsden and Holloway (1992) investigated the energy transfer of small-scale oceanic structures (less than 10 m) including propagating nonlinear internal waves and nonpropagating vortical modes (Riley et al. 1981; Müller et al. 1988; Lelong and Riley 1991). Siegel (1990) also examined the properties of small scales in the ocean but did not address the issues related to resonant interactions.

The goal of this study is to shed light on the following three issues. First, if resonant interactions exist, what are the dominant triads in the ocean? Our investigation of single triads (Lin et al. 1993a) and multiple triads (Lin 1993) shows that the local sum resonant triads dominate and resonant triads of parametric subharmonic instability type are ineffective in energy transfer. We want to check whether or not this is true in an oceanic model spectrum. Second, what kind of interactions will appear in the absence of resonant interactions? Energy transfer from one small-scale mode to another small-scale mode by way of one vertically periodic large-scale mode (induced diffusion; Holloway 1983) is believed to be active although the interactions may not be resonant. The present numerical experiments are set up to verify this conjecture and to learn more about this mechanism. Third, what determines the characteristics of energy transfer? The numerical simulations of multiple triad interactions excited by one energetic mode with white noise (Lin 1993) are consistent with the single triad study (Lin et al. 1993a), suggesting that triad configuration determines the energy transfer pattern. Is this true for the oceanic energy spectrum?

The use of the Garrett–Munk spectrum is to provide a reasonable energy level for each scale. As we know, this spectrum is not designed for small-scale waves, so the results are applied mainly to large- and intermediate-scale waves. The tools we will rely on are bispectrum analysis and phase correlations. These quantities have been used to study nonlinear wave coupling in weakly ionized plasmas (Kim et al. 1980). The cross bispectrum used by Neshyba et al. (1975) was based on the single-station data (temporal information) and revealed no spatial information. The present bispectrum analysis can reveal the distribution of strongly interacting modes in Fourier space. If these modes lie on the resonant traces, interactions are likely to be resonant. In contrast, if the strongly interacting modes do not match the resonant traces, the dominant interactions can be found from the spectral distribution. Phase correlations also provide strong evidence for resonance as resonant triads have approximately constant phase correlations.

2. Numerical method

We consider interactions in a linearly stratified ocean, so the Brunt–Väisälä frequency is constant. The equations that govern the fluid motions include the continuity equation, the incompressible Navier–Stokes equations with the Boussinesq approximation, and the scalar transport equation:

$$u_{i,i} = 0, \tag{2.1}$$

$$u_{i,t} + u_j u_{i,j} = -\frac{p_{,i}}{\rho_0} - \frac{g}{\rho_0}\rho\delta_{i2} + \nu u_{i,jj}, \tag{2.2}$$

$$\rho_{,t} + u_j\rho_{,j} + \frac{d\bar{\rho}}{dx_2}u_2 = \gamma\rho_{,jj}, \tag{2.3}$$

where tensor notation is used in Cartesian coordinates and Einstein summation is invoked. Here u_i, ρ, $\bar{\rho}$, and ρ_0 are the fluctuating velocity, the fluctuating density, background density, and reference density, respectively; x_2 is the vertical axis, ν the kinematic viscosity, γ the molecular diffusivity, and δ_{ij} the Kronecker delta. The Brunt–Väisälä frequency N is

$$\left(-\frac{g}{\rho_0}\frac{d\bar{\rho}}{dx_2}\right)^{1/2}.$$

For computational efficiency, the pseudospectral method is adopted for the spatial derivatives. The Fourier representation implies periodic boundary conditions. Time advancement is based on the second-order Runge–Kutta scheme. The computational domain is normalized to a $2\pi \times 2\pi$ square box resulting in integer wavenumbers, and the inverse Brunt–Väisälä frequency is used to scale time. Prandtl number ($\Pr \equiv \nu/\gamma$) is unity. Noninteger wavenumbers in physical space

are introduced by the stretching factor β_i. When $\beta_i < 1$, physical length scales are increased by a factor of $1/\beta_i$ while wavenumbers are reduced by a factor of β_i, allowing the resolution of very large scale modes. For further details of the numerical method, see Holt et al. (1992) and Lin (1993).

The Garrett–Munk energy spectrum (Munk 1981 referred to as GM79) has been used often. This model spectrum provides a reasonable representation of the oceanic energy distribution for an exponentially stratified ocean. Although in the present work linear stratification is used, energy level is the most important determinant of interaction type. A brief description of this spectrum and its implementation in the code are given in appendixes A and B, respectively. Because this spectrum assumes that the waves are horizontally isotropic, 2D simulations are sufficient to demonstrate the qualitative nature of the dynamic processes (Holloway 1988). The investigation of multiple triad interactions (Lin 1993) also suggests that 2D simulations provide good qualitative results because about 40% of total resonant energy transfer occurs in the vertical plane containing the primary mode and the rest occurs in modes adjacent to these modes.

Before describing our results we need to consider wave–vortex interactions and the role of rotation. Two-dimensional simulations also prohibit wave–vortex interactions that are believed to be significant in energy transfer (Lelong and Riley 1991; Müller et al. 1986). In the study of multiple triad resonant interactions (Lin 1993), this sort of interaction is found. The analysis of the energy distribution shows that if the background white noise consists of internal waves, the wave–vortex interaction is extremely weak. On the other hand, if the white noise is characterized by turbulence, the wave–vortex interaction becomes strong but is still weak compared with the wave–wave resonant interaction. For instance, in the case studied (Lin 1993), only 12% of energy transfer is due to this mechanism and wave–wave interaction is dominant. In addition, this mechanism is active only in the initial phase of interaction, which is contrary to the slow wave–wave interaction. In the present study, all modes are treated as waves, so the wave–vortex interaction should be extremely weak.

Since rotation is excluded in 2D simulations, the results are most applicable to hydrostatic nonrotating waves (Gill 1982). The mesoscale diffusion mechanism (Watson 1985), which is responsible for internal wave energy transport in the f–$2f$ band (f is the inertial frequency), is not investigated. The time unit used in this work is the Brunt–Väisälä period (BVP). The maximum simulation time of 80 BVP corresponds to about 26 hours in an ocean with $N = 5.3 \times 10^{-3}\ \mathrm{s}^{-1}$. If $f = 0.01N$, the inertial wave period is about 33 h, so ignoring rotation is reasonable. The energy in the high wavenumber modes is small and easily dissipated. To avoid aliasing errors and energy accumulation at high wavenumber, a large viscosity equivalent to a small length scale is used. The dissipation could affect the saturated spectral distribution but the dynamics remain qualitatively correct.

A stretching factor $\beta_i < 1$ is used to increase the large-scale (small wavenumber) resolution, especially in the horizontal direction because most of the energy is at small horizontal wavenumber. Two kinds of configurations are used. With $\beta_i = 1$ (cases *od*, *or*, and *oe* of Table 1), about 90% of the total energy is in modes with $k_1 = 0$, implying strong horizontal currents. Although this configuration does not resolve the large-scale modes, it can be used to explore nonlocal interactions between large- and small-scale modes. The second class (cases *yd*, *yr*, and *ye*, Table 1) has $\beta_1 = 1/4$ and $\beta_2 = 1/2$, and 70% of wave energy is in modes with $k_1 = 0$. Simulations of this class were used to do fine-grid verification of the results of the first cases. Finally, cases with smaller energy level (100 times smaller) were performed (Cases *oe* and *ye*) to check Holloway's (1980) argument.

3. Results

a. Energy spectrum evolution

Figure 1a gives the 2D initial kinetic energy spectrum of case *od*. Due to the hydrostatic approximation, the energy of high-frequency modes is very small (appendix B). The energy level decreases rapidly with increasing horizontal wavenumber (k_1) but more slowly with vertical wavenumber (k_2). The very low energy level at high horizontal wavenumber allows a shorter maximum horizontal wavenumber than the vertical one because modes at high k_1 are dissipated rapidly. The highest energy levels are found near $k_1 = 0$ and small k_2 and belong to a strong mean flow. Figure 1b gives the kinetic energy spectrum of case *od* at $t = 10$. It is impossible to identify the dominant energy transfer mechanism from this spectrum. The higher-frequency modes gain energy but remain weak compared with other modes.

TABLE 1. Initial conditions for the 2D simulations: β_i is the stretching factor; c_1 is used to control the total energy level, c_1E_0, where E_0 is the original energy level in GM79; $\hat{u}_i(k_1 = 0) = 0$ with a "Y" denoting that the Fourier components with zero k_1 are set to zero and "N" disables this option. The dimensionless viscosity ν for all cases is 3.95×10^{-6}.

Cases	Mesh size	β_1	β_2	c_1	$\hat{u}_i(k_1 = 0) = 0$
od	64×128	1	1	1	N
or	64×128	1	1	1	Y
oe	64×128	1	1	0.01	N
yd	256×256	1/4	1/2	1	N
yr	256×256	1/4	1/2	1	Y
ye	256×256	1/4	1/2	0.01	N

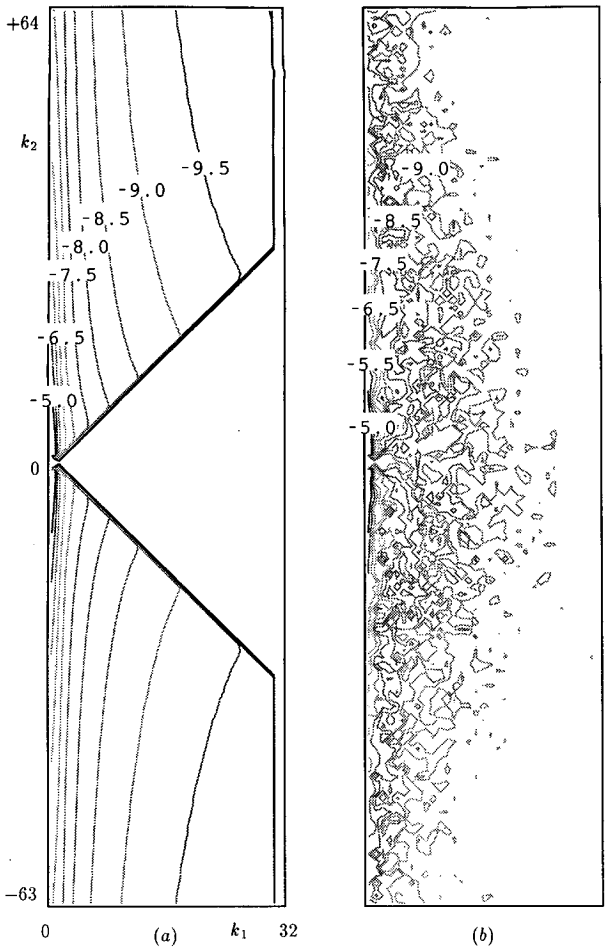

FIG. 1. Kinetic energy spectra of case *od*: (a) $t = 0$; (b) $t = 10$. The label on the figure is obtained from $\log_{10}$ KE.

b. *Bispectrum analysis*

The bispectrum reveals the modes that interact strongly with a chosen mode. Figures 2a–d give the bispectra of case *od* for wavevectors (5, 8), (3, 9), (10, 17), and (3, 14), respectively. Here, (5, 8) and (10, 17) have approximately the same inclination angle (60°), but different wavelengths (9.43 and 19.72) are used to examine the effect of wavelengths. While the inclination angles of (3, 9) and (3, 14) are 72° and 78°, their wavelengths are 9.49 and 14.32, respectively. Accompanied by the former wavevectors, they are used to investigate the effect of the inclination angles of the chosen modes. Since bispectra change slowly with time, those shown are averaged from $t = 0.1$ to 10 BVP. The bispectrum at $t = 80$ is similar to the earlier one and is not shown. For purposes of comparison, the resonant traces are superimposed; these are the loci of modes $\vec{k}^2$ satisfying resonant conditions (Phillips 1977 and Lin et al. 1993a):

$$\Delta\vec{k} = \vec{k}^2 + \vec{k}^3 - \vec{k}^1 = 0 \qquad (3.1)$$

$$\Delta\omega = \omega^2 \pm \omega^3 \pm \omega^1 = 0, \qquad (3.2)$$

where $\vec{k}^1$ is the chosen mode, ω^i is the frequency of wave i ($\omega^i > 0$), and the three wavevectors are not in cyclic form. The solid lines denote sum resonant traces ($\omega^1 = \omega^2 + \omega^3$); the dashed lines are difference resonant traces ($\omega^1 = \mp\omega^2 \pm \omega^3$). There are two small circles in these figures: the lower left one corresponds to the origin and the upper right one locates the chosen wavevector. If resonant interactions dominate, the strongly interacting modes should lie near the resonant traces. In all four cases, the strongly interacting modes do not match the resonant traces but lie on two vertical lines:

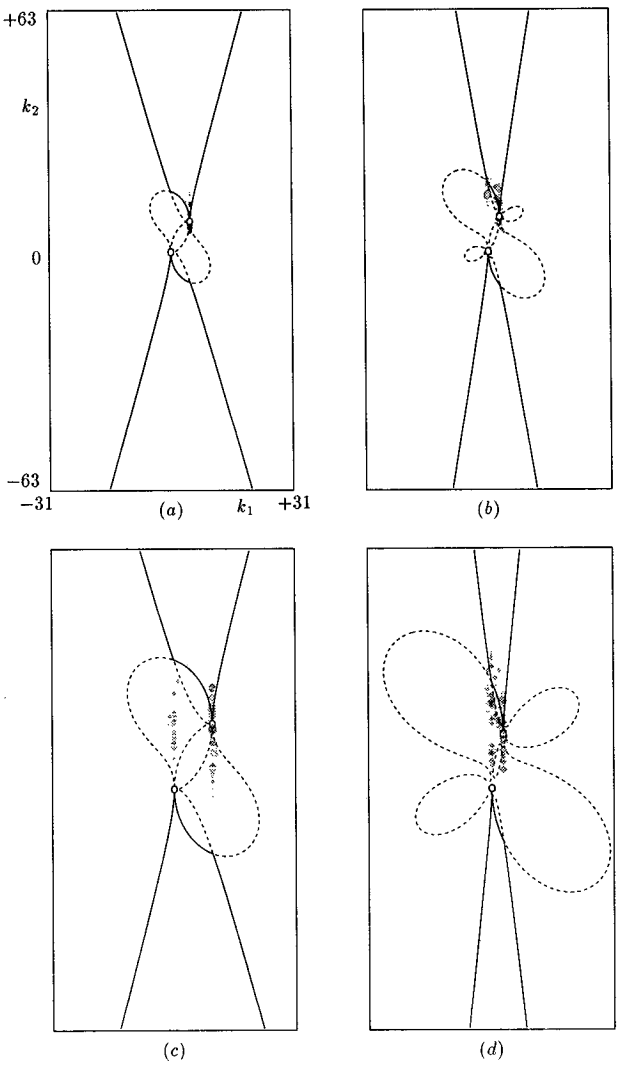

FIG. 2. Time average bispectra from $t = 0.1$ to 10 for case *od* with $\vec{k}$ equal to (a) (5, 8); (b) (3, 9); (c) (10, 17); (d) (3, 14), whose locations are marked by the upper right small empty circle. The lower left small empty circle is the origin. Solid: sum resonant traces; dashed: difference resonant traces.

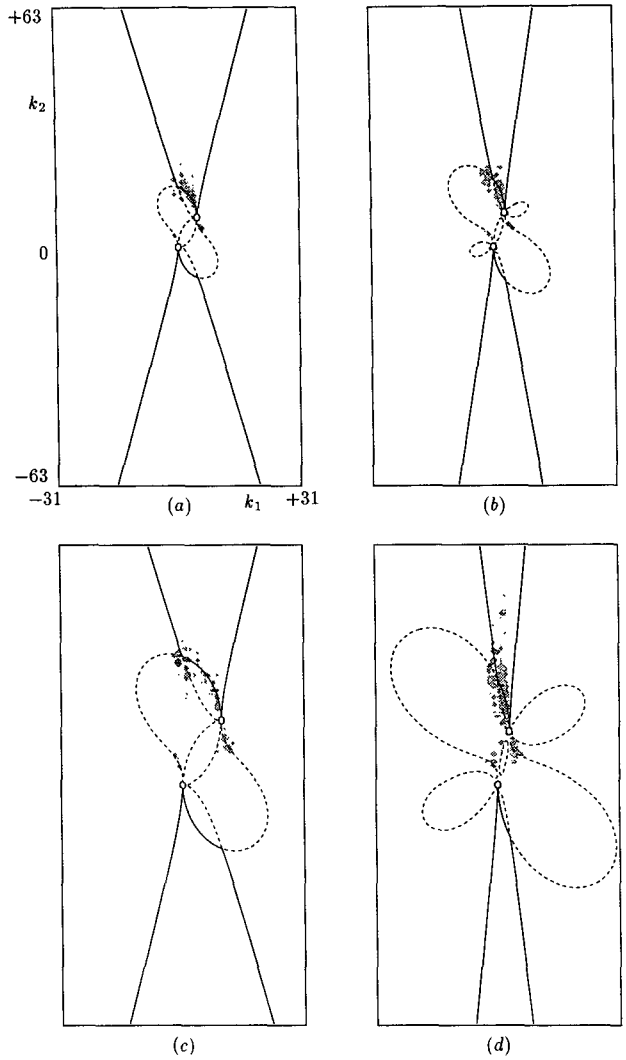

FIG. 3. Time average bispectra from $t = 0.1$ to 10 for case *or* with $\vec{k}$ equal to (a) (5, 8); (b) (3, 9); (c) (10, 17); (d) (3, 14).

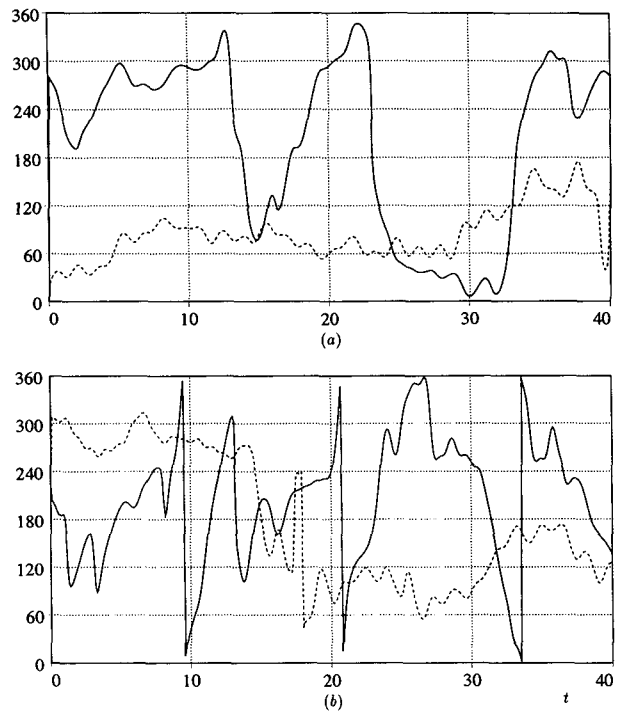

FIG. 4. Time histories of phase correlations for cases *od* and *or*. Solid: case *od*; dotted: case *or*. (a) $\vec{k}^1 = (3, 9)$, $\vec{k}^2 = (2, 14)$; (b) $\vec{k}^1 = (5, 8)$, $\vec{k}^2 = (3, 14)$.

one at $k_1 = 0$ and the other at the horizontal wavenumber of the chosen mode. The former corresponds to mean flow and changes in the energy of these modes indicate modification of the mean profile. The latter are waves resulting from wave–mean flow interaction, which is thus the dominant type of interaction. Recall the critical layer process (Lighthill 1978; Lin et al. 1993b), which is one type of the wave–mean flow interactions: when a wave packet propagates in the direction of increasing mean velocity, the horizontal wavenumber of the wave packet remains unchanged and the vertical wavenumber increases, approaching the critical level asymptotically. It is further found that modes close to the chosen mode are much stronger than those away from it. Therefore, the energy transfer is mainly of the induced diffusion type (McComas and Bretherton 1977) regardless of wavevector orientation and wavelength. Holloway (1983) noted that this mechanism might be effective in energy transfer among finite-amplitude waves. However, the interaction is not resonant as will be demonstrated later.

The dominance of wave–mean flow interactions can be verified by eliminating the mean flow (case *or*). Bispectra for case *or* are shown in Fig. 3 for the same chosen modes as in case *od*. The distribution of the strongly interacting modes approximately matches the resonant traces, implying that the resonant interactions dominate in the absence of mean flow. The interactions are primarily of local sum resonance type (the solid lines); the horizontal wavenumbers of resonant modes $\vec{k}^2$ lie between triads of elastic scattering and induced

TABLE 2. Triads chosen for analysis: $|\Delta\omega|$ is the minimum of $|\omega^1 \pm \omega^2 + \omega^3|$, where wave frequency ω^j is estimated from the linear dispersion relation.

Triad	$\vec{k}^1$	$\vec{k}^2$	$\vec{k}^3$	$\lvert\Delta\omega\rvert$
A	(3, 9)	(2, 14)	(1, −5)	0.02
B	(5, 8)	(3, 14)	(2, −6)	0.004
C	(5, 8)	(5, 9)	(0, −1)	0.044
D	(5, 8)	(3, 21)	(2, −13)	0.237
E	(5, 8)	(8, 23)	(−3, −15)	0.005
F	(5, 8)	(12, 37)	(−7, −29)	0.013
G	(5, 8)	(14, 33)	(−9, −25)	0.199
H	(1, 4)	(0.5, 7)	(0.5, −3)	0.006
I	(1, 4)	(0.5, 9)	(0.5, −5)	0.088

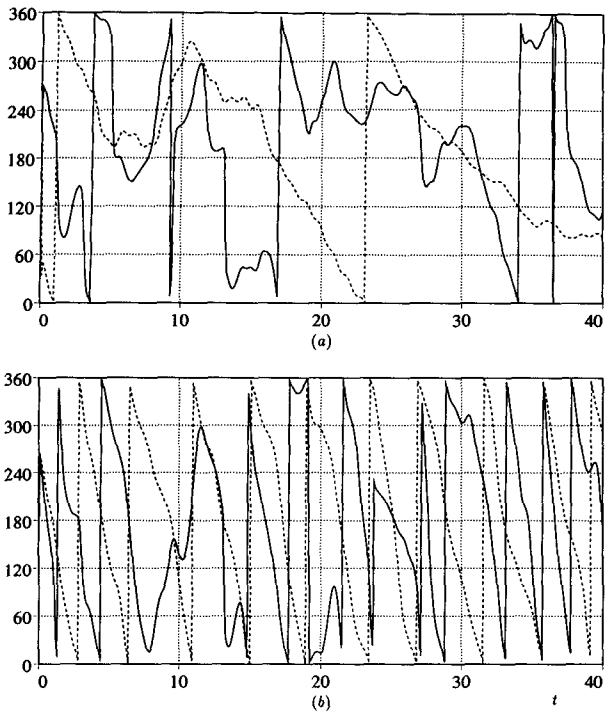

FIG. 5. Time histories of phase correlations of off-resonant triads for cases *od* and *or*. Solid: case *od*, dotted: case *or*. (a) $\vec{k}^1 = (5, 8)$; $\vec{k}^2 = (5, 9)$; (b) $\vec{k}^1 = (5, 8)$, $\vec{k}^2 = (3, 21)$.

diffusion types (Lin et al. 1993a; Lin 1993). The difference resonant modes (dashed lines) are less active. The parametric subharmonic instability (PSI) triad can be constructed by choosing one point along any of the four long legs of the resonant traces and drawing a triangle with respect to the chosen mode. This triad requires that $\kappa^2, \kappa^3 > \kappa^1$, where $\kappa^i = |\vec{k}^i|$. The conventional PSI triad is obtained as the chosen point on the long leg is very far away from the primary chosen mode. Bispectra show that the interactions with small scales are extremely weak, suggesting that PSI triad is not as important as described by McEwan and Robinson (1975), McComas and Bretherton (1977), and Fredericksen (1984). It is characteristic of the GM79 model spectrum that wavevectors of strong modes have large inclination angles and the energy of small-scale modes decreases with increasing wavenumber. As discussed in Lin et al. (1993a) and Lin (1993), a larger inclination angle of the primary wavevector (here the chosen wavevector), smaller white noise amplitude with increasing wavenumber, and triad configuration produce weak PSI interactions. So PSI triads are unlikely to be important in GM79.

The elastic scattering interaction (ES) does not appear in the present cases because of vertical symmetry. If the ES interaction occurs, the mode, whose horizontal wavenumber is of the same as the chosen mode and whose vertical wavenumber is of opposite sign but the same size, should be active. As expected, bispectra indicate that this mode is extremely weak and, therefore, so is the ES interaction.

c. *Phase correlation*

Phase correlation is defined as $\eta^1 \pm \eta^2 \pm \eta^3$, where η^i is the phase of wave i. For resonant triads, the sign depends on the resonance type (sum or difference) and the phase correlation should vary very slowly in time. This analysis is applied to modes on and off the resonant traces. Figures 4a,b give the phase correlations of two triads in cases *od* and *or*. They are triads *A* and *B* in Table 2; both have small $|\Delta\omega|$. The linear resonance condition requires $|\Delta\omega| = 0$. The phase correlations of both triads in case *or* (no mean flow) vary slowly in time, indicating resonance. The triads in case *od* are not resonant because their phase correlations vary rapidly. Clearly, the mean flow in case *od* increases the nonlinearity of the small scales and allows nonresonant interactions to dominate.

We also look at the phase correlations of the off-resonant triads *C* and *D* in Table 2. The former is an induced diffusion (ID) triad with $|\Delta\omega| \approx 0.044$, while the latter has $|\Delta\omega| \approx 0.237$ and its phase correlation should vary rapidly. Figure 5a gives the phase correlations of the ID triad for cases *od* and *or*. It fluctuates with approximate period $1/|\Delta\omega|$ in case *or*, but in

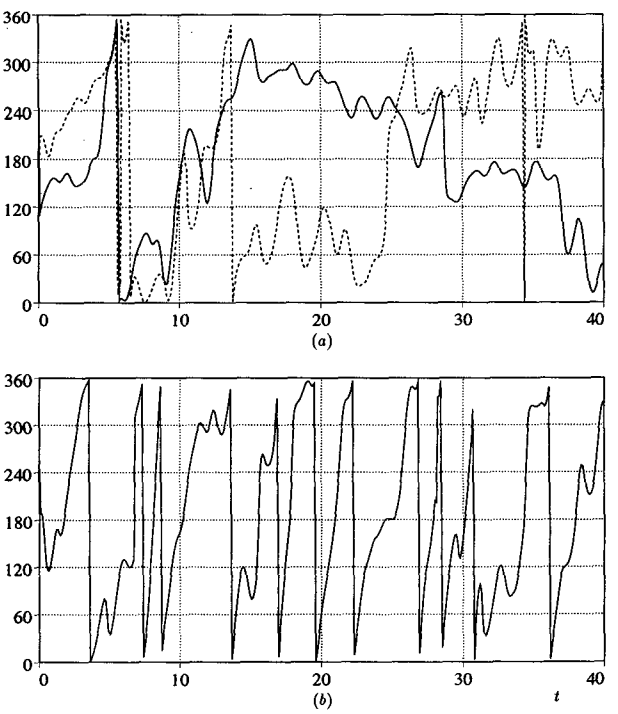

FIG. 6. Time histories of phase correlations for case *or*. (a) Resonant triads with $\vec{k}^1 = (5, 8)$ and $\vec{k}^2$ = solid: (8, 23), dotted: (12, 37). (b) Off-resonant triad with $\vec{k}^1 = (5, 8)$ and $\vec{k}^2 = (14, 33)$.

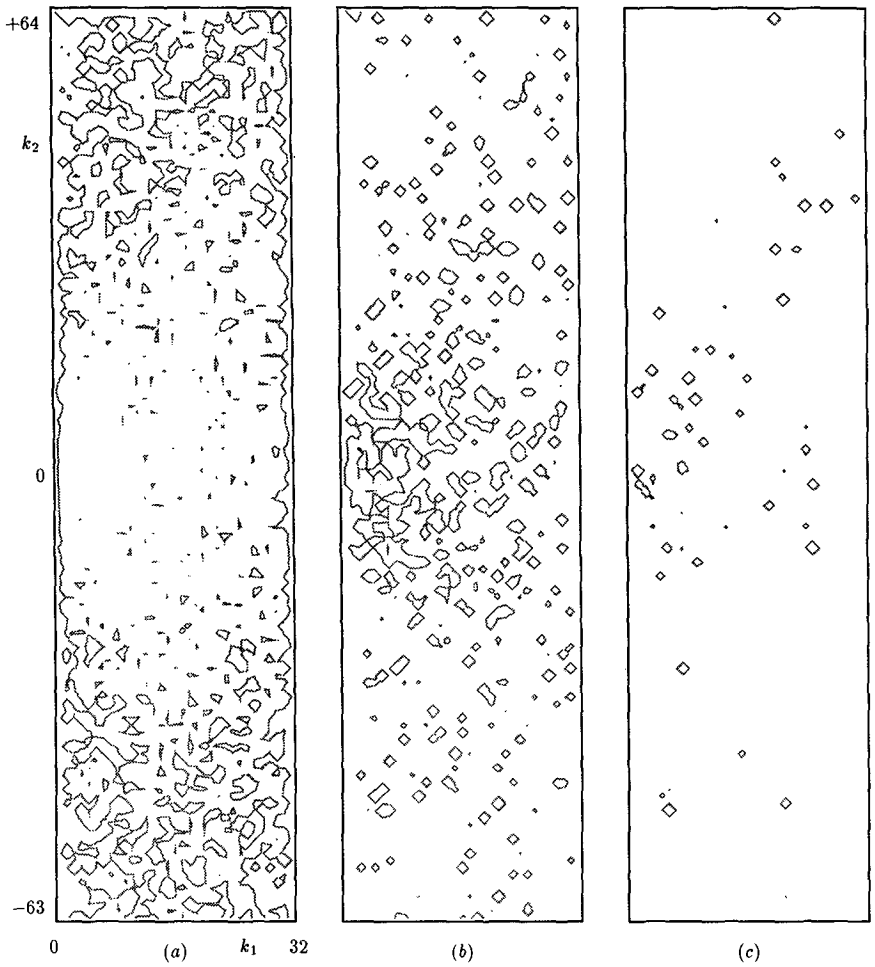

FIG. 7. Contours of T_i/T_w for case *od* at $t = 10$; T_i: interaction timescale and T_w: wave period. Contour levels are (a) 1, (b) 10, and (c) 100.

case *od* the phase correlation is irregular, implying that nonresonant behavior is significant in case *od* but not in case *or*. Figure 5b gives the phase correlations of the second triad with a larger $|\Delta\omega|$. As expected, the phase correlation varies at a higher frequency and is more regular in case *or* than in case *od*.

In section 3b, we used the bispectrum analysis to demonstrate that PSI triads are weak. The question arises as to whether or not they are resonant. To clarify this point, three triads consisting of two long legs and one short leg (the chosen mode) in case *or* are analyzed. They are triads E, F, and G in Table 2. Figure 6a gives the phase correlations of triads E and F in case *or*. For triad E, $\kappa^2 \approx 2.6\kappa^1$; for triad F, $\kappa^2 \approx 4.1\kappa^1$, where $\kappa^i = |\vec{k}^i|$. The variation of the phase correlation suggests that the two triads are resonant. For comparison, the phase correlation of an off-resonant triad with long legs $\kappa^2 \approx 3.8\kappa^1$ (triad G) is plotted as Fig. 6b, which shows that it oscillates much faster than those of triads E and F, confirming the resonance in triads E and F. So in the absence of mean flow the chosen mode resonates with the small-scale modes, but energy transfer is very weak.

In summary, the phase correlations of triads involving strong mean flow but satisfying linear resonant conditions oscillate rapidly, indicating that the presence of strong mean currents tend to weaken resonant interactions; this is consistent with bispectrum analysis. Energy transfer to small-scale modes by parametric subharmonic instability is very weak regardless of resonance.

d. Interaction timescale versus wave period

The ratio of interaction timescale to wave period has been used by McComas and Bretherton (1977) and McComas and Müller (1981) to indicate the applicability of weak interaction theory to the ocean. However, Holloway (1980) questioned this and found that their results contradict the weak interaction as-

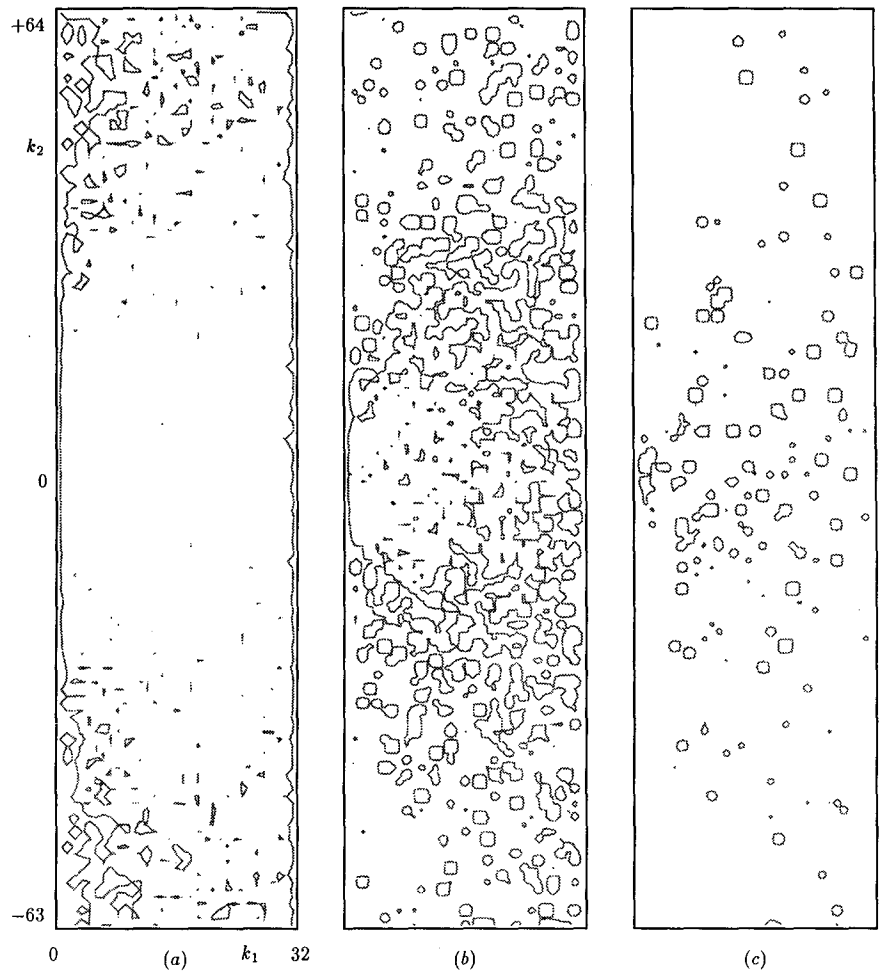

FIG. 8. Contours of T_i/T_w for case *or* at $t = 10$; T_i: interaction time scale and T_w: wave period. Contour levels are (a) 1, (b) 10, and (c) 100.

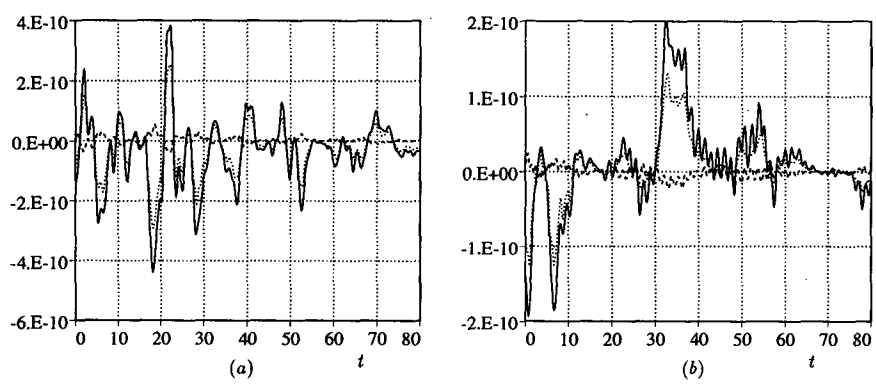

FIG. 9. Total energy transfer rates (T^{ij}) of a local triad; ij = 12 (solid), 13 (dashed), and 23 (dotted). Triad wavevectors are $\vec{k}^1 = (5, 8)$, $\vec{k}^2 = (3, 14)$, $\vec{k}^3 = (2, -6)$ for (a) case *od* and (b) case *or*.

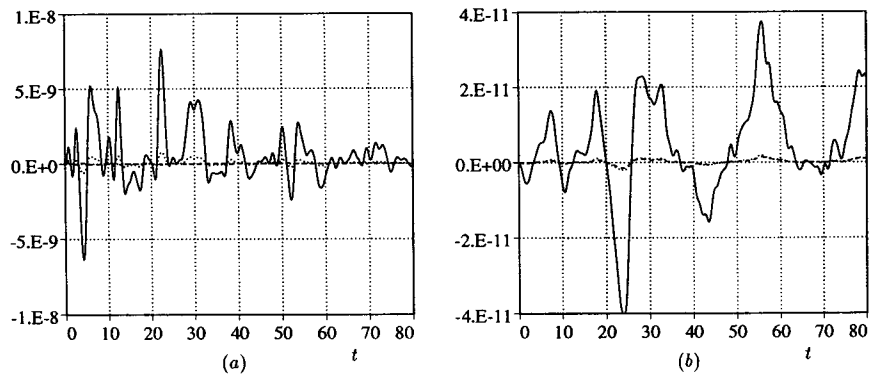

FIG. 10. Total energy transfer rates (T^{ij}) of slightly off-resonant triads of ID type; ij = 12 (solid), 13 (dashed), and 23 (dotted). Triad wavevectors are $\vec{k}^1$ = (5, 8), $\vec{k}^2$ = (5, 9) and $\vec{k}^3$ = (0, −1) for (a) case *od* and (b) case *or*.

sumption. Since, from the previous studies, case *od* is dominated by nonresonant interactions while case *or* is dominated by resonant interactions, investigating the timescale ratios of the two cases can shed light on the significance of this ratio. The contours of the timescale ratios for cases *od* and *or* are shown in Figs. 7 and 8, respectively. The interaction timescale (T_i) and wave period (T_ω) are defined as

$$T_i \equiv |E/(dE/dt)|, \tag{3.3}$$

$$T_w \equiv 1/\omega, \tag{3.4}$$

where E and dE/dt are energy and energy transfer rate, respectively, and ω is the wave frequency. Resonant interactions require that the ratio T_i/T_w be large. Three contour levels are shown: 1, 10, and 100. Since the contours look similar all the time, data at t = 10 are used. For case *od*, a small ratio occurs at low frequency and a high ratio is found in the high-frequency region, implying that wave frequency affects the timescale ratio. The ratio is small over a large portion of the GM79 energy spectrum, especially at high wavenumber and low frequency, suggesting that these modes are unlikely to interact resonantly.

Since resonant interactions occur in case *or*, more modes should have large timescale ratios. Figure 8 gives the contours of the timescale ratio. Contour level 1 (Fig. 8a) is less likely and contour levels 10 and 100 are more likely compared with case *od* (Fig. 7), so resonant interactions are more common. Although the contour density is qualitatively consistent with the bispectrum analysis, it is hard to say how big the timescale ratio must be before interactions can be called weakly resonant. Furthermore, active triads cannot be identified by the ratios.

e. Energy transfer analysis

In this section, the energy flow pattern is analyzed in order to compare with single triad analysis (Lin et al. 1993a) and numerical investigations of multiple triad interactions excited by a single energetic wave (Lin 1993). The total energy transfer rate (T^{ij}), which

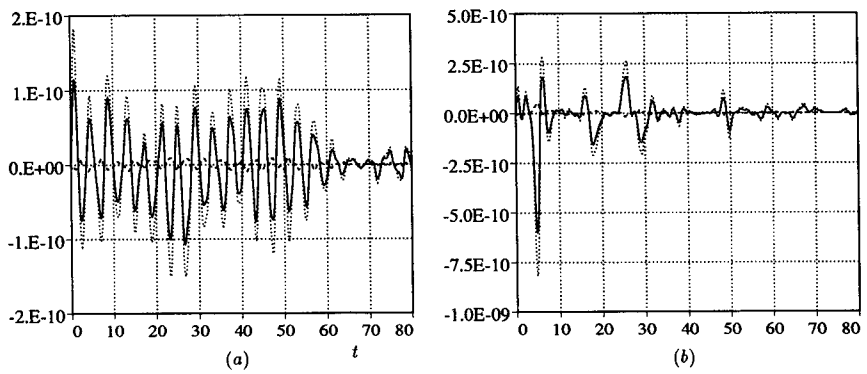

FIG. 11. Total energy transfer rates (T^{ij}) of off-resonant triads; ij = 12 (solid), 13 (dashed), and 23 (dotted). Triad wavevectors are $\vec{k}^1$ = (5, 8), $\vec{k}^2$ = (3, 21) and $\vec{k}^3$ = (2, −13) for (a) case *or* and (b) case *od*.

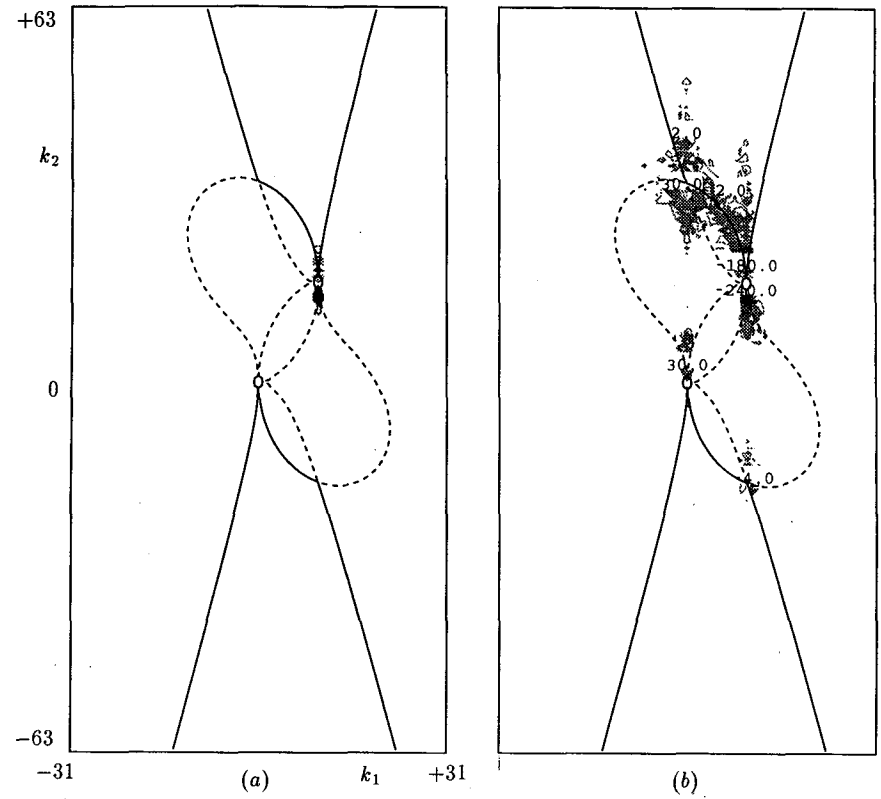

FIG. 12. Time average bispectra from $t = 0.1$ to 10 for case *oe* with different contour levels. The chosen wavenumber is (10, 17): (a) high contour level and (b) small contour level [30 times small than that of (a)].

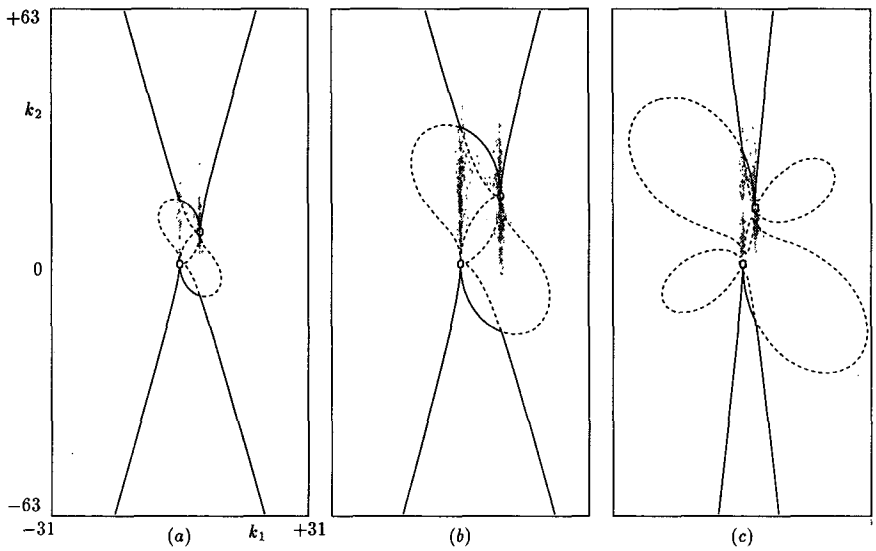

FIG. 13. Time average bispectra from $t = 0.1$ to 10 for Case *yd* with $\bar{k}$ equal to (a) (5, 8); (b) (10, 17); (c) (3, 14).

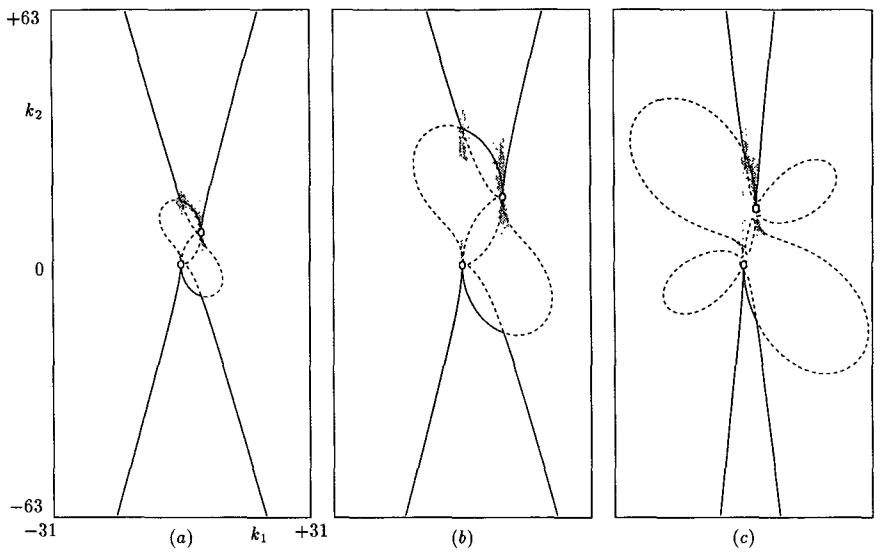

FIG. 14. Time average bispectra from $t = 0.1$ to 10 for case *yr* with $\vec{k}$ equal to (a) (5, 8), (b) (10, 17), and (c) (3, 14).

is defined as rate of total energy transfer from wave i to wave j, is analyzed. The analyzed triad has $\vec{k}^1 = (5, 8)$, $\vec{k}^2 = (3, 14)$, and $\vec{k}^3 = (2, -6)$ (triad B in Table 2, approximately satisfying linear resonance conditions). Figures 9a,b are time histories of the total energy transfer rates for cases *od* and *or*, respectively. The energy transfer in the two cases seems to be different, but a particular pattern can be found in the two cases. Energy is taken from mode $\vec{k}^1$ by mode $\vec{k}^2$, then transferred to mode $\vec{k}^3$, and finally back to mode $\vec{k}^1$, or vice versa; it is cyclic. The energy transfer pattern is as predicted by the analysis of a resonant interaction coefficient, which depends solely on the triad structure (Lin et al. 1993a) and is similar to the energy transfer in the multiple triad interactions (Lin 1993). The dynamic similarities between cases with strong and weak nonlinearity and with different initial spectra [GM79 and a single energetic mode with white noise in Lin (1993)] suggest that triad configuration is the principal determinant of energy transfer pattern.

The total energy transfer rates of two other triads in cases *od* and *or* are analyzed. One is triad C in table 2, which is of induced diffusion (ID) type and slightly off-resonant. The other is triad D in Table 2, which does not satisfy linear resonance conditions and has a large $|\Delta\omega|$. The total energy transfer rates of the ID triad in cases *od* and *or* are shown in Figs. 10a,b, respectively. The interactions between modes $\vec{k}^1$ and $\vec{k}^2$, which have about the same length scales, are much stronger than the interactions with the mean flow (mode $\vec{k}^3$), consistent with the single and multiple triad interaction results (Lin et al. 1993a; Lin 1993). Furthermore, the interactions in case *od* are about 100 times stronger than in case *or*, indicating that induced diffusion is enhanced by the presence of a mean flow. In this energy transfer mechanism, the mean flow does not gain or lose much energy from the other modes, but its strength determines the rates of energy transfer between the two small-scale modes. For the off-resonant triad D in case *or*, the energy transfer behaves as expected; energy is transferred back and forth among modes but there is no long time average energy transfer (Fig. 11a). In case *od*, the pattern is not clear due to strong nonlinearity (Fig. 11b). This suggests that, in the absence of mean flow, resonant interactions dominate; however, in general, mean flow increases the nonlinearity of the small scales, invalidating weak interaction theory.

f. Effect of reduced energy level

Holloway (1980) argued that oceanic waves are about 100 times too strong to be treated as weak waves. In case *oe* (Table 1), the energy level is reduced by a factor of 100 to see whether resonance occurs. Figures 12a,b show bispectra for chosen mode $\vec{k} = (10, 17)$, which is a typical mode representative of the other modes. The contour level in Fig. 12a is 30 times the level in Fig. 12b to show strongly interacting modes. Figure 12a shows that the strongly interacting modes have the same horizontal wavenumber as the chosen mode, indicating dominance of wave–mean flow interactions. These interacting modes become stronger as they are close to the primary mode. Thus, triads of induced diffusion type have the strongest interaction. However, they are not resonant. When the contour levels are reduced by a factor of $\sim$30, modes on the linear resonant traces appear, indicating that resonant interactions exist but are weak. Triads of the parametric subharmonic instability type are not found; their role

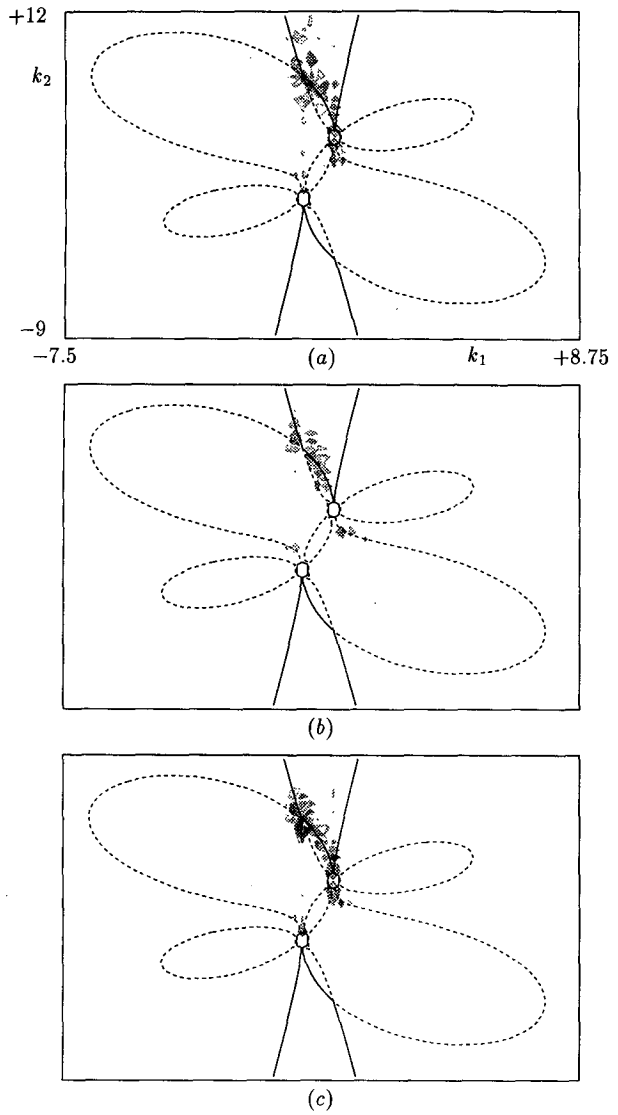

FIG. 15. Time average bispectra from $t = 0.1$ to 10 with $\vec{k} = (1, 4)$ for case (a) *yd*, (b) *yr*, and (c) *ye*. The horizontal axis is increased by a factor of 2 to enhance visualization.

in the oceanic energy distribution may have been overemphasized by McEwan and Robinson (1975) and McComas and Bretherton (1977). Overall, as the total energy level of GM79 is reduced, more resonant interactions occur but nonresonant interactions remain active at high wavenumber. The vertical wavelength of the chosen mode $\vec{k} = (10, 17)$ corresponds to about 70 m and resonant interactions are weak at this scale.

g. *Fine grid test*

In the cases above, the number of large-scale modes is limited. In this section, stretching factors are employed to increase the number of small wavenumber modes; the horizontal (β_1) and vertical (β_2) stretching factors are 1/4 and 1/2. Cases *yd*, *yr*, and *ye* (Table 1) correspond to the unstretched cases *od*, *or*, and *oe*, respectively. Wave amplitudes with $k_1 = 0$ are set to zero in case *yr*, leaving only about 30% of the original total energy. In case *ye*, the energy level is reduced by a factor of 100.

Bispectra for cases *yd* and *yr* are shown in Figs. 13 and 14, respectively, for chosen modes $\vec{k} = (5, 8), (10, 17)$, and $(3, 14)$. In case *yd* the strongly interacting modes do not match the resonant traces, and wave–mean flow interactions dominate. In case *yr*, interactions with chosen modes $\vec{k} = (5, 8)$ and $(3, 14)$ are resonant but interactions with small scales, like $\vec{k} = (10, 17)$, are dominated by wave–mean flow interactions; this differs from case *or* (Fig. 3c) and occurs because the increased number of large-scale modes increases the nonlinearity of the small-scale modes. The bispectra of the three chosen modes for case *ye* are similar to those of case *yr*, indicating that resonance is unlikely to occur at small-scale modes. It is expected that if more large-scale modes are included, resonant interactions between large and small scales are even more unlikely.

We also examined the bispectrum of a large-scale mode $\vec{k} = (1, 4)$, whose vertical wavelength is about 300 m. Its bispectra for cases *yd*, *yr*, and *ye* are given in Figs. 15a–c. The horizontal axis has been stretched by a factor of 2 to enhance visualization. The interactions are local and there is no sign of parametric subharmonic instability. The active modes are mainly of local sum resonance type (solid lines) but there are a few local difference resonant modes (dashed lines). Thus large scale modes (in the present cases, vertical wavelength about 300 m) can be resonant, even for case *yd* in which GM79 is used without modification, qualitatively consistent with Holloway's proposal (1983). Recall the bispectrum for $\vec{k} = (5, 8)$ (case *yd*, Fig. 13a), in which nonresonant wave–mean flow interactions dominate. Its vertical wavelength is 150 m, half that of mode $\vec{k} = (1, 4)$. So modes with vertical wavelength between 150 and 300 m can transfer energy via both resonant and nonresonant interactions.

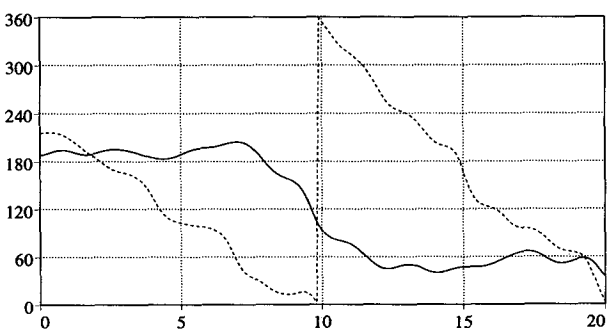

FIG. 16. Time histories of phase correlations for case *yd* with $\vec{k}^1 = (1, 4)$ and $\vec{k}^2$ equal to solid: (0.5, 7), and dashed: (0.5, 9).

Since the nature of the resonance in case *yd* (Fig. 15a) is not as clear as in the other cases, two triads are chosen for phase correlation analysis: one is resonant triad *H* (Table 2) and the other is slightly off-resonant triad *I*. Figure 16 gives the phase correlations. The first triad has slowly varying phase correlation, implying resonance. In the second triad, the phase correlation varies at approximate frequency $1/|\Delta\omega|$. This is consistent with the bispectrum analysis and indicates that local sum resonant interactions are active for large scales in GM79.

4. Discussion

Three issues are addressed in this work. The first is to determine the dominant resonant triads in a model ocean. The second is to discover the energy transfer mechanism when resonant interactions are not strong. The third is to explore the role of triad configuration in energy transfer pattern. These issues were studied by using direct numerical simulations and a Garrett–Munk initial spectrum. The tools used to identify resonant interactions include bispectrum analysis and phase correlation. When the distribution of strongly interacting modes matches the linear resonant traces, resonant interactions are active. As further confirmation of the existence of resonance, the phase correlation of a resonant triad should be a weak function of time.

It was found that resonant interactions occur at small wavenumbers (corresponding to vertical wavelength greater than 150 m in GM79); the dominant resonant interactions are of local sum type. Parametric subharmonic instability triads do not play a significant role due to small interaction coefficients, decreasing energy level with increasing wavenumber and the large inclination angles of the strong modes. Resonance is limited to very large scales [qualitatively consistent with Holloway's (1983) proposal]. Most of the GM79 model spectrum is governed by wave–mean flow interactions, among which the triad of the induced diffusion type is most effective. The high wavenumber modes are weak enough for resonance, but the strong mean current increases nonlinearity and resonance is destroyed. The similarity of energy transfer patterns in weak and strong interactions and in different energy spectra suggests that triad configuration almost alone governs the energy flow pattern within a triad. Reducing the energy level by a factor of 100 is not enough to make the very small scales resonant. Finally, we conclude that resonant interactions exist, but do not dominate in the GM79 model spectrum.

In summary, we verified and found numerically the following.

- At very large scale modes, resonant interactions occur. Triads of local sum resonance type are active while interactions with very small scale modes (PSI triads) are weak. So PSI triads seem to be unimportant in GM79.
- At intermediate and small-scale waves, wave–mean flow interactions dominate. Among them, induced diffusion interaction is the strongest.
- The similarity of energy flow pattern between nonresonant and resonant triads suggests that triad configuration determines the characteristics of energy transfer.

Acknowledgments. The authors would like to thank Professors Stephen Monismith, Sanjiva Lele, Jorg Imberger, and Hidekatsu Yamazaki for valuable discussions. This work was supported by the Small Scale Physical Oceanography Program at the Office of Naval Research under Grant N00014-89-J-1909. The computations were performed on the Cray Y-MP at the NAVOCEANO Supercomputer Center.

APPENDIX A

Features of Garrett–Munk Spectrum

The Garrett–Munk oceanic energy spectrum described in Munk (1981, referred to as GM79) is used as the initial conditions. The GM spectrum is presented in frequency and vertical wavenumber space and is based upon an exponentially stratified ocean. The normalization factors are the reference buoyancy frequency ($N_0 \approx 5.2 \times 10^{-3}$ s^{-1}) and the *e*-folding length scale [$b = 1.3$ km is the depth at which $N = N_0 e^{-1}$; Garrett and Munk (1972)]. In GM79, the energy contribution of the vertical fluctuating velocity is set to zero so the hydrostatic approximation is applicable. Moreover, if the Coriolis frequency (f) equals zero, the kinetic and potential energy are equipartitioned. GM79 gives the following expression:

$$E(\omega, j) = B(\omega)H(j)E_0 \tag{A1}$$

$$B(\omega) = \frac{2}{\pi}\frac{f}{\omega(\omega^2 - f^2)^{1/2}} \tag{A2}$$

$$H(j) = \frac{(j^2 + j_*^2)^{-1}}{\sum_{j=1}^{\infty}(j^2 + j_*^2)^{-1}}, \tag{A3}$$

where $f = 7.3 \times 10^{-5}$ s^{-1}, $E_0 = 6.3 \times 10^{-5}$ and

$$\int_f^N B(\omega)d\omega = 1 \tag{A4}$$

$$\sum_{j=1}^{\infty} H(j) = 1, \quad j_* = 3; \tag{A5}$$

j is the index of the vertical wavenumber as will be explained later: $B(\omega)$ and $H(j)$ are to fit observed properties of oceanic energy spectrum, and $B(\omega)$ is chosen to fit the moored spectra in the ocean and allows for the peak at the inertial frequency [Eq. (A2) is singular at $\omega = f$]. Most of the energy resides in the large vertical scale modes due to the function $H(j)$ [Eq.

(A3)]. For example, if j_* in Eq. (A3) is set to 3, more than half of the energy is contained in modes with $j \leq 3$. The relation between j and the vertical wavenumber (κ_2) is (Munk 1981)

$$k_2 b = j\pi\left(\frac{N^2-\omega^2}{N_0^2-\omega^2}\right)^{1/2} \approx j\pi\frac{N}{N_0}, \quad \text{if } N \gg \omega > f, \quad \text{(A6)}$$

where $k_2 b$ is the normalized vertical wavenumber. Since the hydrostatic approximation is invoked, the wavenumber restriction $0 \leq k_1 \leq k_2(1-f^2/N^2)^{1/2}$ is imposed.

APPENDIX B

Implementation

For the present purpose, the spectrum has to be transformed to the wavenumber space and the dispersion relation under the hydrodynamic approximation

$$\omega^2 = N^2\left(\frac{k_1}{k_2}\right)^2 + f^2 \quad \text{(B1)}$$

is invoked. Since a constant buoyancy frequency is used, the relation between j and the vertical wavenumber [Eq. (A6)] is reduced to $k_2 = j\pi$ (note that k_2 denotes the normalized vertical wavenumber, hereafter). Thus, the transformation relation (Garrett and Munk 1975) is

$$E(k_1, k_2) = E(\omega, k_2)\frac{d\omega}{dk_2} = E(\omega, k_2)\left(\frac{N}{k_2}\right)^2\frac{k_1}{\omega}. \quad \text{(B2)}$$

In the above relation, the normalized k_2 is used instead of j; therefore, $H(j)$ [Eq. (A3)] is rearranged to be

$$H(k_2) = \frac{(k_2^2 + k_{2*}^2)^{-1}}{\sum_{k_2=\pi}^{\infty}(k_2^2 + k_{2*}^2)^{-1}}. \quad \text{(B3)}$$

After transformation, GM79 becomes

$$E(k_1, k_2) = E_0\frac{2}{\pi}\frac{Nfk_2}{N^2k_1^2 + f^2k_2^2}H(k_2). \quad \text{(B4)}$$

We should be aware that the above formula is continuous in k_1 and discrete in k_2, so

$$E_0 = \int_{k_1=0}^{\infty}\sum_{k_2=\pi}^{\infty}E(k_1, k_2)dk_1. \quad \text{(B5)}$$

As we see, GM79 is continuous in k_1 and singular at frequency f [Eq. (A2)] so that E approaches a very large value as k_1 goes to zero, indicating that the total energy level would be much greater than E_0 if GM79 expression [Eq. (B4)] is applied to a discrete k_1 system, like the present simulation. The resolution for this problem is to integrate Eq. (B4) in k_1 from $k_1 = k_{1s}$ to $k_1 = k_{1e}$ and use the energy spectrum obtained, which is

$$E(k_{1s} : k_{1e}, k_2) = E_0\frac{2}{\pi}H(k_2)\left[\arctan\left(\frac{Nk_{1e}}{fk_2}\right) - \arctan\left(\frac{Nk_{1s}}{fk_2}\right)\right]. \quad \text{(B6)}$$

Since the wavenumber is integer, for an unstretched case, $(k_1 - 0.5)$ and $(k_1 + 0.5)$ are chosen for k_{1s} and k_{1e}, respectively, and $E(k_{1s} : k_{1e}, k_2)$ is used to represent energy at the wavenumber (k_1, k_2) in a discrete wavenumber system. At $k_1 = 0$, $k_{1s} = 0$ and $k_{1e} = 0.5$ are used instead. By this way, the total energy level remains unchanged; that is,

$$E_0 = \sum_{k_1=0}^{\infty}\sum_{k_2=1}^{\infty}E(k_{1s} : k_{1e}, k_2). \quad \text{(B7)}$$

After normalization, the parameters become as follows:

$$N = 1, \quad f = 1.404 \times 10^{-2}, E_0 = 2.487 \times 10^{-3}.$$

Since Munk (1981) stated that E_0 is universal and is within a factor of 2, an E_0, which is one-half of the original (1.2435×10^{-3}), is used to keep the energy level as low as possible. Those modes that do not satisfy the wavenumber restriction $0 \leq k_1 \leq k_2(1-f^2/N^2)^{1/2}$ are assigned a very small energy level (10^{-12}).

REFERENCES

Flatté, S. M., F. S. Henyey, and J. A. Wright, 1985: Eikonal calculations of short wavelength internal wave spectra. *J. Geophys. Res.*, **90**(C4), 7265–7272.

Fredericksen, J., 1984: Interactions of nonlinear internal gravity waves and turbulence. *Ann. Geophys.*, **2**, 421–432.

Garrett, C., and W. Munk, 1972: Space-time scales of internal waves. *Geophys. Fluid Dyna.* **2**, 225–264.

——, and ——, 1975: Space-time scales of internal waves: A progress report. *J. Geophys. Res.*, **80**(3), 291–297.

——, and ——, 1979: Internal waves in the ocean. *Ann. Rev. Fluid Mech.*, **11**, 339–369.

Gill, A., 1982: *Atmosphere-Ocean Dynamics.* Academic Press.

Hasselmann, K., 1966: Feynman diagrams and interaction rules of wave-wave scattering processes. *Rev. Geophys.*, **4**, 1–32.

——, 1967: A criterion for nonlinear wave instability. *J. Fluid Mech.*, **30**(4), 737–739.

Holloway, G., 1980: Oceanic internal waves are not weak waves. *J. Phys. Oceanogr.*, **10**, 906–914.

——, 1982: On interaction time scales of oceanic internal waves. *J. Phys. Oceanogr.*, **12**, 293–296.

——, 1983: A conjecture relating oceanic internal waves and small-scale processes. *Atmos. Ocean*, **21**(1), 107–122.

——, 1988: The buoyancy flux from internal gravity wave breaking. *Dyn. Atmos. Oceans*, **12**, 107–125.

Holt, S. E., J. R. Koseff, and J. H. Ferziger, 1992: A numerical study of the evolution and structure of homogeneous stably stratified sheared turbulence. *J. Fluid Mech.*, **237**, 499–539.

Kim, Y. C., J. M. Beall, J. Powers, and R. W. Miksad, 1980: Bispectrum and nonlinear wave coupling. *Phys. Fluids*, **23**(2), 258–263.

Lelong, M.-P., and J. J. Riley, 1991: Internal wave-vortical mode interactions in strongly stratified flows. *J. Fluid Mech.*, **232**, 1–19.

Lighthill, J., 1978: *Waves in Fluids.* Cambridge University Press.

Lin, C.-L., 1993: Multiple triad resonant interactions in linearly stratified fluids. *J. Fluid Mech.*, submitted.

——, J. H. Ferziger, J. R. Koseff, and S. G. Monismith, 1993a: Single triad resonant interactions in linearly stratified fluids. *J. Fluid Mech.* submitted.

——, ——, ——, and ——, 1993b: Simulation and stability of two-dimensional internal gravity waves in a stratified shear flow. *Dyn. Atmos. Oceans*, **19**, 325–366.

Martin, S., W. Simmons, and C. Wunsch, 1972: The excitation of resonant triads by single internal waves. *J. Fluid Mech.*, **53**, 17–44.

McComas, C. H., 1977: Equilibrium mechanisms within the oceanic internal wave field. *J. Phys. Oceanogr.*, **7**, 835–845.

——, and F. P. Bretherton, 1977: Resonant interaction of oceanic internal waves. *J. Geophys. Res.*, **82**(9), 1397–1411.

——, and P. Müller, 1981: Time scales of resonant interactions among oceanic internal waves. *J. Phys. Oceanogr.*, **11**, 139–147.

McEwan, A. D., and R. M. Robinson, 1975: Parametric instability of internal gravity waves. *J. Fluid Mech.*, **67**(4), 667–687.

Müller, P., G. Holloway, F. Henyey, and N. Pomphrey, 1986: Nonlinear interactions among internal gravity waves. *Rev. Geophys.* **24**(3), 493–536.

——, R.-C., Lien, and R. Williams, 1988: Estimates of potential vorticity at small scales in the ocean. *J. Phys. Oceanogr.*, **18**, 401–416.

Munk, W. H., 1981: Internal waves and small-scale processes. *Evolution of Physical Oceanography,* Warren, B. A. and C. Wunsch, Eds., The MIT Press, 264–291.

Neshyba, S., and E. J. C. Sobey, 1975: Vertical cross coherence and cross bispectra between internal waves measured in a multiple-layered ocean. *J. Geophys. Res.*, **80**(9), 1152–1162.

Olbers, D. J., 1976: Nonlinear energy transfer and the energy balance of the internal wave field in the deep ocean. *J. Fluid Mech.*, **74**(2), 375–399.

Phillips, O. M., 1977: *The Dynamics of the Upper Ocean.* Cambridge University Press.

Pomphrey, N., J. D. Meiss, and K. M. Watson, 1980: Description of nonlinear internal wave interactions using Langevin methods. *J. Geophys. Res.*, **85**(C2), 1085–1094.

Ramsden, D. and G. Holloway, 1992: Energy transfers across an internal wave-vortical mode spectrum. *J. Geophys. Res.*, **97**(C3), 3659–3668.

Riley, J. J., R. W. Metcalfe, and M. A. Weissman, 1981: Direct numerical simulations of homogeneous turbulence in density-stratified fluids. *Nonlinear Properties of Internal Waves,* B. J. West, Ed., Amer. Institute Phys., 79–112.

Shen, C. Y., and G. Holloway, 1986: A numerical study of the frequency and the energetics of nonlinear internal gravity waves. *J. Geophys. Res.*, **91**(C1), 953–973.

Siegel, D. A., and J. A. Domaradzki, 1990: Three-dimensional simulation of a decaying internal wave field. *J. Phys. Oceanogr.*, submitted.

Watson, K. M., 1985: Interaction between internal waves and mesoscale flow. *J. Phys. Oceanogr.*, **15**, 1296–1311.